Received: 30 June 2020 | Revised: 25 September 2020 | Accepted: 28 September 2020

DOI: 10.1111/gcb.15397

PRIMARY ARTICLE

Global Change Biology WILEY

Direct response of tree growth to soil water and its implications for terrestrial carbon cycle modelling

Annemarie H. Eckes-Shephard[1] | Egor Tiavlovsky[2] | Yizhao Chen[1] | Patrick Fonti[3] | Andrew D. Friend[1]

[1]Department of Geography, University of Cambridge, Cambridge, UK

[2]10 Sovereign Place, Apollo Way, Cambridge, UK

[3]Swiss Federal Institute for Forest, Snow and Landscape Research, Birmensdorf, Switzerland

Correspondence
Annemarie H. Eckes‐Shephard, Department of Geography, University of Cambridge, Downing Place, Cambridge CB2 3EN, UK.
Email: ahe24@cam.ac.uk

Funding information
A.D.F., P.F. and Y.C. acknowledge support from the Natural Environment Research Council under grant NE/P011462/1. P.F. also acknowledges support from the Swiss National Science Foundation (projects INTEGRAL-121859, LOTFOR-150205 and CLIMWOOD-160077).

Abstract

Wood growth constitutes the main process for long-term atmospheric carbon sequestration in vegetation. However, our understanding of the process of wood growth and its response to environmental drivers is limited. Current dynamic global vegetation models (DGVMs) are mainly photosynthesis-driven and thus do not explicitly include a direct environmental effect on tree growth. However, physiological evidence suggests that, to realistically model vegetation carbon allocation under increased climatic stressors, it is crucial to treat growth responses independently from photosynthesis. A plausible growth response function suitable for global simulations in DGVMs has been lacking. Here, we present the first soil water-growth response function and parameter range for deciduous and evergreen conifers. The response curve was calibrated against European larch and Norway spruce in a dry temperate forest in the Swiss Alps. We present a new data-driven approach based on a combination of tree ring width (TRW) records, growing season length and simulated subdaily soil hydrology to parameterize ring width increment simulations. We found that a simple linear response function, with an intercept at zero moisture stress, used in growth simulations reproduced 62.3% and 59.4% of observed TRW variability for larch and spruce respectively and, importantly, the response function slope was much steeper than literature values for soil moisture effects on photosynthesis and stomatal conductance. Specifically, we found stem growth stops at soil moisture potentials of −0.47 MPa for larch and −0.66 MPa for spruce, whereas photosynthesis in trees continues down to −1.2 MPa or lower, depending on species and measurement method. These results are strong evidence that the response functions of source and sink processes are indeed very different in trees, and need to be considered separately to correctly assess vegetation responses to environmental change. The results provide a parameterization for the explicit representation of growth responses to soil water in vegetation models.

KEYWORDS

Larix decidua Mill., *Picea abies* (L.) H. Karst, soil moisture, soil moisture growth response, source–sink, tree growth, tree physiology, tree rings, vegetation modelling, xylogenesis

1 | INTRODUCTION

Trees sequester CO_2 long-term through biomass formation. Globally, more than three trillion trees (Crowther et al., 2015) sequester about 18% of annual anthropogenic emissions (Le Quéré et al., 2018; Pan et al., 2011) in their stems. Wood growth is therefore a crucial process in maintaining the climate mitigation effect of terrestrial ecosystems. Tree ring width (TRW) is the indicator of annual stem radial increment. Variable TRWs at environmentally limiting sites provide important long-term evidence of how tree growth responds to the environment (Douglass, 1914) and simultaneously how much carbon was captured in the stem. However, despite tree rings being used to reconstruct climate through correlation, our mechanistic understanding of growth processes and their environmental drivers remains limited (Cuny et al., 2015).

1.1 | The need for representing growth (sink) – Processes in global vegetation models

Future vegetation response to climate change is typically modelled using dynamic global vegetation models (DGVMs). These models simulate the dynamic carbon stocks of global vegetation in a 'source-centric' manner, emphasizing environmental limitations on photosynthesis (Fatichi et al., 2019), the carbon input into the plant. Growth (sink-) processes, the demand of carbon by different organs, are treated by DGVMs and the majority of forest growth models with simple rules, rather than explicit consideration of the environmental controls on the sinks (e.g. see Merganičová et al., 2019). As a result, most DGVMs estimate plant growth as a more-or-less linear function of the outcome of the supply of carbon through photosynthesis. However, growth itself is under direct environmental control, such as through water limitations, and not only determined by the amount of available carbon (Fatichi et al., 2014; Körner, 2006, 2015). For example, abrupt responses to decreasing soil moisture have been reported for growth, but not photosynthesis, in a number of species (Bogeat-Triboulot et al., 2007; Boyer, 1970; Hummel et al., 2010; Lempereur et al., 2015; Tardieu et al., 1999; Wardlaw, 1990), uncoupling these two processes (Muller et al., 2011). Explicit representation of wood growth in DGVMs has been argued for by Fatichi et al. (2019), Friend et al. (2019), and Zuidema et al. (2018). However, existing attempts to mechanistically represent stem growth either treat these as marginal processes besides main processes studied or too complex to be applied in a global modelling context. For example, Génard et al. (2001) focus on the shrinkage and swelling in the stem. Their simulated growth increment was not very sensitive to growth rate or cell wall extensibility, but highly sensitive to the threshold value of irreversible growth (wall-yielding threshold pressure parameter). Other growth modelling approaches, e.g. Steppe et al. (2006) largely focus on stem water storage and sapflow variations, which make them overly complex for a stem increment model in a DGVM. Hoölttä et al. (2010) further increase complexity by modelling sugar and water-driven growth of all cells in the developing ring in a small tree segment. While much can be learned from such detailed mechanistic frameworks, a simpler approach representing first-order growth responses to water limitations has to be used for ring width increment modelling in DGVMs, to remain sufficiently efficient.

1.2 | Existing studies may not be easily extrapolated to natural ecosystems

To our knowledge, there are only two studies describing a first-order response curve type relationship between tree ring increment and soil moisture (Bogeat-Triboulot et al. [2007]: on drought-adapted 2 month old *Populus euphratica* Oliv. plantlets in a greenhouse experiment; Lempereur et al. [2015]: on mature coppiced evergreen oak in the Mediterranean). Both studies report an abrupt decline of growth in response to decreasing predawn (Lempereur et al., 2015) or midday (Bogeat-Triboulot et al., 2007) soil water conditions, with Lempereur et al. (2015) reporting specific values of soil water potential below which ring increment ceases (<1.1 MPa) for evergreen oak. However, as both experiments were performed on drought-adapted species and under artificial conditions, their results may not be directly relevant to other tree species or natural ecosystems.

Increased understanding of the relationship between growth and soil water is therefore required, especially for mechanistically modelling growth responses under climate change, as there is a projected increase in hydrological stress in many forest ecosystems of the world (Allen et al., 2015; Brzostek et al., 2014).

1.3 | Deriving tree growth response curves from existing observations

Existing observations have the potential to be used for deriving response curve relationships. Tree rings are the most numerous and long-term data on climate-growth responses, including drought. Many studies link radial growth increment in form of TRW or BAI to hydrological variables such as precipitation (e.g. Hughes et al., 1994) or -more commonly- monthly drought indices (Ljungqvist et al. [2020] discusses many of them). So far, the few studies on soil moisture variations associated with TRWs (e.g. Brzostek et al., 2014; Kharuk et al., 2017) or intra-annually resolved observations with dendrometers (e.g. Downes et al., 1999; Eilmann et al., 2011; Giovannelli et al., 2007; Zweifel et al., 2006) remain correlative and thereby only imply underlying mechanisms. However, these co-varying features between soil moisture and growth increment can also be used to derive physiologically meaningful response curves that can be used to model growth. While dendrometer data are more accurate, instantaneous and have been successfully applied to this purpose in Lempereur et al. (2015), ring widths are readily available, numerous, cover large areas and long

time periods. While final TRWs usually lack information at the intra-seasonal resolution of growth processes, xylogenesis observations (e.g. Cuny et al.., 2012) and/or sites with reliable growing seasons can be used to narrow down the biologically meaningful period of growth. However, soil moisture observations for correspondingly long periods do not exist. Nevertheless, with simulated soil moisture (e.g. Lempereur et al., 2015) and reasonably approximated annual growth period length, it may be possible to use ring widths directly to establish physiologically meaningful growth response functions and thresholds. This goes beyond the correlative approaches usually applied in disciplines such as dendroclimatology.

1.4 | A novel TRW-based approach to generate soil moisture response curves

Our goals in this study are (a) to find the optimal parameterization for a soil moisture growth response curve that can reproduce observations of soil moisture-driven ring width variations at our study site; and (b) to compare this response curve with existing source and sink response curves from published observational and modelling studies. These goals are addressed through the following questions:

1. What is the relationship between daily tree ring increment and daily predawn soil moisture?
2. How does the response curve compare with those for leaf-level (photosynthesis and stomatal conductance) processes?
3. What does this imply for the effect of soil moisture deficit on tree growth and how to model it?

First, we verified the new individual-based vegetation-hydrology framework in HYBRID9 (an updated version of HYBRID8 (Ekici et al., 2015)) based on its performance on various timescales and hydrological outputs. We then used HYBRID9 to simulate a century of soil moisture dynamics forced by CRUNCEP (7.2) gridded data (0.5° resolution; Viovy, 2018), with downscaled temperature and precipitation. After ensuring that ring width increment at our study site in the Swiss Alps is primarily water limited, we determined a common intra-annual critical period during which growth most frequently occurs for all years. We represented a soil water-growth response curve as a bounded linear function together with a daily additive growth model and used a data-driven approach based on observed TRWs to optimize for the best soil water-growth parametric relationship. The resulting growth (sink) response functions and their parameters are compared against growth response functions and thresholds from existing observational studies, as well as source response functions used in DGVMs.

We define growth, or ring width increment, as a combination of cumulative cell proliferation and enlargement activity. Our soil water response curve thus represents the impact of both these processes, and does not distinguish between the two. This definition focuses on the volume, not mass increase of the tree.

2 | METHODS

2.1 | Model description

HYBRID9 is an individual-based DGVM. Updates are a revised soil hydrology framework based on the Community Land Model (CLM) 4.5 (Oleson et al., 2013). The CLM soil hydrology framework used by HYBRID9 contains eight layers of soil, concluded with an aquifer at the bottom. Processes represented are infiltration, surface and subsurface runoff, diffusion, gravity drainage, root fraction-dependent transpiration and ground-water interactions (Oleson et al., 2013). A tridiagonal system of equations is applied to solve for vertical water flow, which is represented following Zeng and Decker (2009). HYBRID9 differs from the CLM approach through the omission of a full energy budget and the following assumptions. Evapotranspiration is partitioned between canopy and soil surface using the approach of Shuttleworth and Wallace (1985). A simple one-layer representation of snowpack dynamics is included. The framework continues the principle of a coupled photosynthesis-conductance scheme from HYBRID3 (Friend et al., 1997), where soil moisture effects on stomatal openness impact carbon assimilation as well as transpiration. Rooting distribution is modelled for each individual using the two-parameter root distribution model for temperate forest data developed by Schenk and Jackson (2002), with the root fraction in each model layer subsequently calculated according to eq.(16) in Amenu and Kumar (2008). Full details of the HYBRID9 hydrology framework are included in Supporting Information S1.

2.2 | Study site description

The study site is located at 804 m above sea level (a.s.l.) on a north facing slope above the village of Gampel (46°30′26″N, 7°74′11″W), within the inner-alpine Swiss Rhône valley (Canton Valais; see Figure S1). The selected site is the lowest of an elevational growth monitoring network located along the forested slopes around Lötschental (see King et al., 2013, for the network description). The climate is continental with a mean annual temperature of 9.6°C and an annual precipitation of 604 mm (data for the period 1980–2019 from MeteoSwiss weather station of Visp, 639 m a.s.l., 10 km west of the study site). The summer months are usually dry due to warm day temperatures (average 25–23°C from June to September) and low precipitation (43 mm/month). The soils are formed from calcareous-free substrate, including moraines and crystalline bedrock (gneiss and granite), and are part of the Aar massif. This causes acidic soils characterized by coarse stone content and low amounts of clay, which hence may drain freely. The forest at the site is a mixture of *Larix decidua* Mill, *Picea abies* L. (H) Karst and *Pinus sylvestris* L., which are 120–180 years old and 20–25 m in height.

2.3 | Tree ring chronologies

In 2012 and 2016, 16 mature, healthy dominant trees of both larch (*L. decidua* Mill) and spruce (*P. abies* L. (H) Karst) were selected for ring width measurements. This selection also included trees for which growth had been monitored over 2008–2010, with weekly micro-coring performed during the growing season. Increment borers were used to obtain 5 mm diameter radial cores per tree stem at breast height, perpendicular to the slope to avoid reaction wood (data available from Cuny et al., 2019). Standard dendrochronological techniques were used to prepare, measure and cross-date TRW series of each species. Ring widths were measured along the core using the Linear table (LINTAB, Rinntech, Heidelberg Germany) and COFECHA (Grissino-Mayer, 2001) for a statistically-based quality control of the visual cross-dating (see Supporting Information S6.1 for chronology construction).

2.4 | Soil moisture measurements

Soil volumetric water content (vvol) was measured hourly from July 2008 to 2016 using 10 sensors (EC-5; Decagon), inserted at 10 and 70 cm depths, distributed over two locations within the study site (see Peters et al., 2019, for more details).

2.5 | Spatial downscaling of climate data

We needed to simulate long-term soil moisture dynamics for the site to drive our soil moisture growth response parameterization framework. For this we required relatively accurate long-term climate forcing for the site. As no long-term daily climate observations were available near our study site, we spatially downscaled the CRUNCEP half-degree gridded dataproduct which contained our site. This was necessary because this particular gridcell's topography and hence local climate is very heterogeneous. For our site, the gridded data product overestimates precipitation by 1,307.0 mm/year, and underestimates temperature by 7.5°C (see Table S1). Using local observations over 2006–2016, we applied the delta method to downscale gridded temperature and empirical quantile mapping to downscale gridded precipitation (see Supporting Information S3). Having downscaled the data, we were able to simulate long-term soil moisture dynamics in HYBRID9, after a few parameter alterations.

2.6 | Parameter selection

Model parameters were adjusted to the local stand and soil structure (see Supporting Information S5). To reflect the site's tree age and height, trees were grown in the model from a range of random initial radii no larger than 0.01 m from 1805 and at a density of 36 individuals per 200 m^2. In 1900 they had reached a mean height of 22 m, which is then assumed the equilibrium height of the managed stand. From then on, trees were kept at a constant height of 22 m, and had reached a maximum density of eight individuals per 200 m^2.

2.7 | HYBRID9 model evaluation

To evaluate how well HYBRID9 simulates soil moisture, we applied Spearman correlation. To evaluate seasonal correspondence, root mean square deviations between modelled (L3 and L6) and observed (−10 cm and −70 cm) volumetric water content content were calculated on a daily, monthly and yearly basis. Volumetric water content was used to calibrate HYBRID9 soil hydrology dynamics (updated parameters in Table S4). The then calibrated HYBRID9 soil hydrology also produces soil water potential (Ψ_{soil}) outputs that were the relevant moisture variable for this study. We also compared an 8 day aggregated HYBRID9 total surface evaporation (evaporation and transpiration) to compare with the 8 day moderate resolution imaging spectroradiometer (MODIS) evapotranspiration product (Running et al., 2017). The MODIS product was taken from the closest available coordinates (46°29′N, 7°75′W).

2.8 | Dendroclimatic analysis

To ensure that the site is only water limited and establish the period during which soil moisture statistically impacts final TRW, we applied a daily-resolution correlation approach following aspects from Kaczka et al. (2017). The residual chronologies (see Supporting Information S6.1) for larch and spruce were correlated with several (environmental) variables, such as simulated vvol (mm^3/mm^3), simulated Ψ_{soil} (MPa) and downscaled precipitation (mm/day) and temperature (°C). Analyses were restricted to layer 4 (i.e. between 16.6 and 28.9 cm below ground), because modelled rooting density is highest there. Briefly, linear correlation coefficients were computed between final TRW values and environmental variables aggregated over time intervals of all possible daily durations (from 1 to 365 days) and starting dates within the calendar year (total of 66,795 coefficients computed; Kaczka et al., 2017) For water-related variables, our significance cutoff was <0.05, for temperature, <0.1.

2.9 | Defining the growth period

To select the period of tree growth (critical period between onset (t_1) and cessation (t_2) expressed as Julian day), we used three sources of evidence: xylogenesis data are the main source, which is supported by the daily-resolution climate correlation approach for growth cessation (t_2), and by a growing degree-day (GDD) model to confirm growth onsets across the century (t_1; Figure 1; see Supporting Information S7 for more detailed description of the methods).

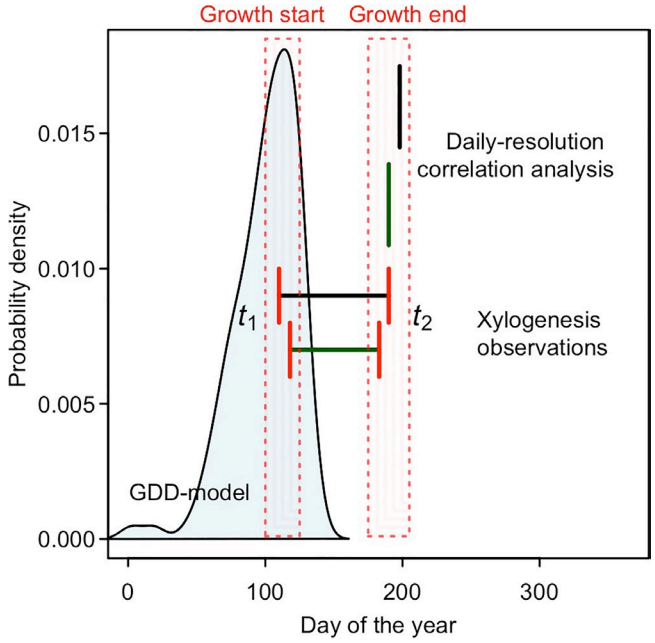

FIGURE 1 Schematic for the definition of growth period. Horizontal lines terminated by red vertical lines show the growth duration for larch (green) and spruce (black), as derived from xylogenesis observations. Growth increment start (t_1) is defined as the first Julian Day at which the radial files of 3 years of xylogenesis observations had more than 50% of the observed radial files display at least one enlarging cell (Rathgeber et al., 2011). Additionally, growth increment start for all 116 years was modelled using the CLM5.0 growing degree-days equation for cold leaf-out timing (equation 1, section 2.29.12.1.1 [Lawrence et al., 2019]), thereafter called 'GDD-model' (light-blue density distribution curve). t_1 values derived from xylogenesis data were then located within the probability density distribution (see left red-highlighted section). Growth increment cessation (t_2) is defined as the first Julian day at which the first tree during 2008–2010 was reported to no longer have enlarging cells. Growth cessation based on daily-resolution correlation analysis (last day during which correlation predawn Ψ_{soil} and tree ring width index is observed) is shown as green (larch) and black (spruce) single vertical lines. For dates used in further analysis, we adhere to the conservative results from the xylogenesis analysis and for growth start subtract 7 days to account for cambial activity before enlargement. For exact dates, see Table 2

2.10 | The relationship between annual ring width increment and soil moisture variations

We derived a threshold parameter for growth from Ψ_{soil}-sensitive simulations of tree rings which provided the best match with tree ring observations.

The simplest description of the relationship between soil water potential and β_{growth} (relative ring width increment; unitless) can be given by a one parametric response curve in the shape of a bounded linear function between 1 and 0 (Equation 1).

$$\beta_{growth}(\Psi_{soil}) = \begin{cases} \frac{\psi_{crit} - \Psi_{soil}}{\psi_{crit}}, & \text{if } \psi_{crit} < \Psi_{soil} \leq 0 \\ 0, & \text{if } \Psi_{soil} \leq \psi_{crit}, \end{cases} \quad (1)$$

where ψ_{crit} is a parameter (MPa) and Ψ_{soil} is soil water potential (MPa). The soil water response factor, β_{growth} varies in response to the daily predawn soil water potential in soil layer 4 for larch and soil layer 3 for spruce, to account for the difference in rooting depth and exploit the more root-dense soil layers as predicted by HYBRID9.

Before simulating tree rings for comparison with tree ring width index (TRWi) data, we first binned the observed TRWi data into 11 bins (see Figure S8) and computed the average value in each bin ($TRWi_b$). By averaging we expect the variability due to unsystematic effects to cancel out. We hypothesize that the only remaining dominant effect causing the difference in averaged growth between bins will be due to variation in Ψ_{soil} histories given that water is the main driver of between-year variability in tree growth (TRWi) at this site (Figure 4). For binning, we used a clustered binning approach (Equation 2; Section S8) to avoid separation of very similar TRWi values by a percentile boundary. In this approach, breaks were set between clusters of data points (TRWis) which are assumed to be more similar to each other because they have grown under more similar soil water regimes. Each bin was constrained to contain at least six samples, but final numbers vary depending on the similarity of TRWi values (see Figure S8). As the sample numbers in these 'clustered' bins are unequal, subsequent analysis may be sensitive to outliers in bins with few samples. We accounted for this in our objective function (i.e. Equation 5). Using a clustered binning approach, we could set more biologically sensible locations for bin breaks between TRWis. We clustered the observed TRWi in bins and preserved the sets of year indices belonging to each bin. We then used the same bin-specific sets of year indices to aggregate and average the predicted TRWs values in corresponding bins:

$$TRWi_b = \frac{1}{n_b} \sum_{y \in \text{bin b}} TRWi_y. \quad (2)$$

In order to simulate growth, we assume the following relationship between individual year Ψ_{soil} time series (indexed by y) and corresponding simulated tree ring width ($TRWs_y$) for a given ψ_{crit}:

$$TRWs_y(a) = \sum_{t=start}^{t=end} a \times \beta_{growth}(\Psi_{soil\ y}(t)) = a \times \sum_{t=start}^{t=end} \beta_{growth}(\Psi_{soil\ y}(t)) = a \times \overline{TRWs}_y, \quad (3)$$

where $\beta_{growth}(\Psi_{soil\ y}(t))$ is the nonlinear function from Equation (1) parameterized by ψ_{crit}, t is a given day of the growth period. Scaling coefficient 'a' is species-specific and taken to be the same for all years. It is calibrated below in relation to detrended observed TRWi values, along with the response function parameter ψ_{crit}. Start and end dates for the critical growth period are species-specific parameters identified in our critical period analysis. In this growth model we make the assumption that there is no growth for any $TRWs_y$ in the absence of any favourable moisture conditions during the growing season.

For direct comparison with $TRWi_b$, we average individual yearly simulated $TRWs_y$ in each bin (b):

$$TRWs_b(a) = \frac{1}{n_b} y \text{ bin b} \in \sum TRWs_y(a) = a \times \frac{1}{n_b} y \text{ bin b} \in \sum \overline{TRWs}_y = a \times \overline{TRWs}_b, \quad (4)$$

where n_b is number of samples in bin b.

We gradually decrease ψ_{crit} from 0 to −4.6 MPa. For each setting of ψ_{crit} we compute $\overline{TRWs}_b$ values. For the fixed $\overline{TRWs}_b$ values we then vary a to minimize the sum of weighted residual squared errors (SWRSE) between simulated and observed binned TRW values:

$$SWRSE(a) = \sum_{b=1}^{n_{bins}} n_b \times (TRWs_b(a) - TRWi_b)^2 = \sum_{b=1}^{n_{bins}} n_b \times (a \times \overline{TRWs}_b - TRWi_b)^2. \quad (5)$$

We report the R^2 measure which is derived directly from SWRSE and quantifies in relative terms how much variation in observed $TRWi_b$ values is reproduced using our proposed model relationship between Ψ_{soil} histories and final TRW growth (Equation 2). Minimum SWRSE corresponds to maximum R^2,

$$R^2(a) = 1 - \frac{SWRSE(a)}{\sum_{b=1}^{n_{bins}} n_b \times (TRWi_b - mean(TRWi))^2}, \quad (6)$$

$$\text{with } mean(TRWi) = \frac{1}{N} \sum_{b=1}^{b=M} n_b \times TRWi_b, \quad (7)$$

where M is the number of bins, and N is total number of samples (years, and $TRWi_b$ are observed bin averages.

For each setting of ψ_{crit} there is a corresponding value of a which maximizes the R^2 objective above. We call it $\hat{a}(\psi_{crit})$. Figure 5b,f shows the values of objective function $R^2(\hat{a}(\psi_{crit}))$ for a range of ψ_{crit} values (grey dots).

We select the pair $(\psi^*_{crit}), a^* = \hat{a}(\psi^*_{crit})$ for which the above R^2 objective is maximized globally (see Table 3).

To verify that our optimization procedure found the optimal setting for ψ_{crit} subject to the chosen model relationship in Equation (3), we fix the optimized parameter a^*, simulate corresponding $\overline{TRWs}_b$ under varying ψ_{crit} and compute $R^2(a^*)$. The resulting maxima coincide for the global optimal value of a, which verifies that our optimization procedure did indeed find the optimal ψ_{crit} value.

3 | RESULTS

3.1 | HYBRID9 model evaluation

HYBRID9 hydrology output was evaluated for its accuracy in simulating soil moisture dynamics, to make sure that it could be used for soil moisture-growth response analyses. Observed and modelled soil moisture from 2008 to 2016 for the two soil depths (−10 and −70 cm) are shown in Figure 2.

At both depths, observed and modelled soil water content show a similar seasonal pattern with high soil moisture during the winter, decrease in late spring and lowest values during the summer (July). For the majority of time, modelled soil moisture dynamics are located within the range of observations (purple shaded area) with good correspondences, independently of the climatic data used (nearby station data (green lines) or downscaled CRUNCEP). Spearman correlations with CRUNCEP are 0.62 for the upper layer and 0.78 at 70 cm depth, and are consistent over different time scales, from day to year (Table 1). Analysis of variance shows the lowest root mean squared error (RMSE) for both layers in the annual analysis (0.020 mm^3/mm^3), and highest variance for layer 3 (0.040 mm^3/mm^3) for daily comparison. The lower correspondence at 10 cm depth is due to spikes in soil water content which do not always coincide in time. These spikes are less prominent at 70 cm depth.

HYBRID9 captures the multi-year decreasing soil moisture trend in the period over 2008–2015, as well as the temporary recovery to 2008 levels in 2012. In the last years (i.e. 2014–2016), modelled

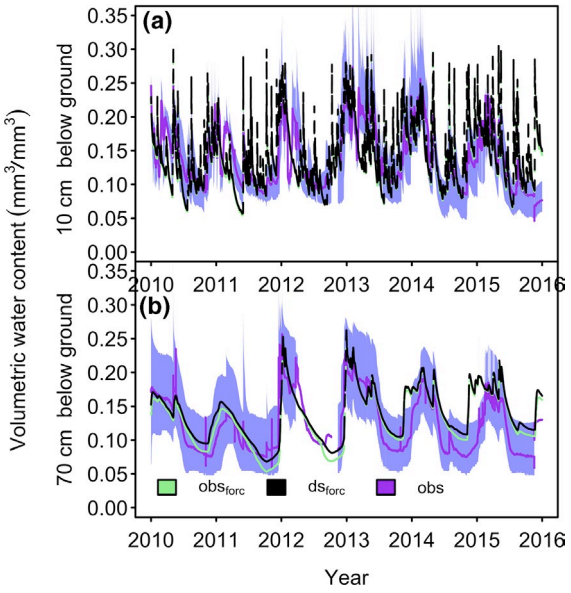

FIGURE 2 Soil moisture dynamics at two different depths (−10 cm [a] and −70 cm [b]) over 2008–2016, with observed soil moisture together with its upper and lower observed bounds, (from mid 2008–2016), and two outputs from HYBRID9: obs_{forc} is forced with a combination of default CRUNCEP gridded data products (air specific humidity [g/g], incoming shortwave radiation [W/m^2 × 21,600], incoming long wave radiation [W/m^2], pressure [Pa]) and local observations on precipitation (mm/day) and temperature (°K); ds_{forc} is forced by a combination of default CRUNCEP (see above) and downscaled precipitation and temperature gridded data products based on the local observations. Observed soil moisture is denoted in purple (with maximum of $n = 4$, the mean is embedded in purple shade which is the max and min value of observed values at that depth; where $n = 1$, only a single value is available, which is directly plotted instead of the mean)

TABLE 1 Comparison of observed and modelled soil moisture. Correlation coefficients (Spearman) and root mean square deviations between modelled (L3 and L6) and mean observed (−10 cm and −70 cm) volumetric soil moisture content over different time periods. ρ = Spearman's rank correlation coefficient

	ρ	RMSE daily	RMSE monthly	RMSE yearly
Layer 3	0.620	0.041	0.036	0.020
Layer 6	0.778	0.037	0.033	0.022

soil moisture at −70 cm continues to increase during November and December, whereas these dynamics are delayed to January in the observations. While the period of high soil moisture content is shorter for the observed than for the modelled soil moisture, the magnitudes continue to be similar and within the range of observations. These results give confidence that the model is able to capture the major features at all timescales of soil moisture variation characteristics at both depths.

Figure 3 shows the evaporation dynamics of HYBRID9 and the MODIS product over 2008–2016. Timing and magnitude between HYBRID9 and MODIS are similar, with the exception of the late summer, where the MODIS product is higher in later years than HYBRID9 during some summer periods. Overall, however, MODIS and HYBRID9 total surface evaporation dynamics behave in a similar manner in terms of both magnitude and timing. We conclude that modelled soil moisture is sufficiently robust to be used for accurately simulating soil moisture-growth responses at daily resolution over the century.

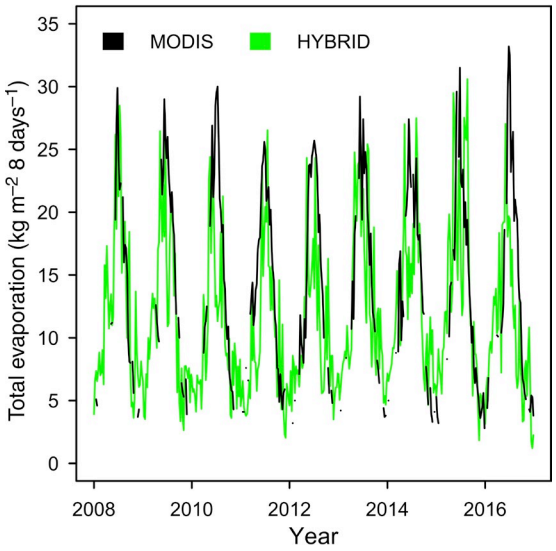

FIGURE 3 Comparison of the summed soil surface evaporation and evapotranspiration of HYBRID9 (8 day aggregate) and the MODIS evapotranspiration product

3.2 | Dendroclimatic analysis

Figure 4 shows the daily climate correlation analysis results between larch or spruce TRWi and downscaled precipitation and temperature, and modelled volumetric water content (vvol) and soil water potential.

Correlation between annual ring width and moisture-related variables are significant ($p < .05$) in spring and early summer and generally follow the same pattern throughout the year. Predawn soil water potential almost continuously correlates well with ring width when starting from February for larch, or early March for spruce until the end of June (DOY 190) for larch and early July (DOY 198) for spruce. Maximum correlations for soil water potential-TRW are $r = .300$ and .350 for larch and spruce respectively. No duration starting from DOY 198 for spruce and DOY 190 for larch shows any correlation between any moisture variable and TRWi. For larch the signal returns in mid-August, for about two weeks.

Negative correlation with TRW and rainfall is observed in August for larch and spruce, with the effect having a longer-lasting impact on spruce (almost 4 months). The correlation signal is also detectable in volumetic water content and soil water potential for spruce 1–2 months later.

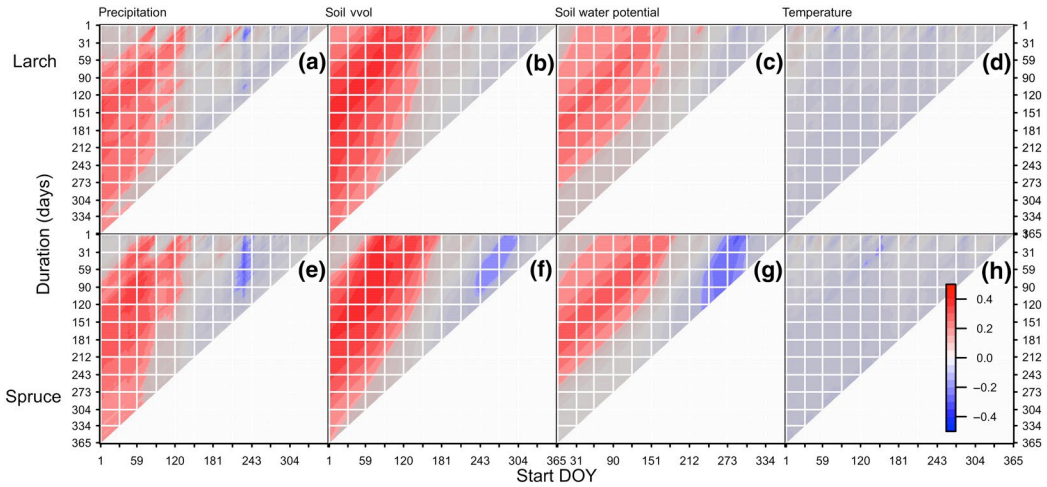

FIGURE 4 Daily-resolution correlation analysis for the whole year between spruce or larch tree ring width index and environmental variables. (a)/(e) precipitation, (b)/(f) modelled predawn soil volumetric water content (vvol) in layer 4, (c)/(g) modelled predawn soil water potential in layer 4, and (d)/(h) temperature. Predawn modelled values are model output from 06:00 a.m. All values with $p > .05$ for (a)–(c), (e)–(g) and $p > .1$ for (d)/(h) are shaded in grey. The *x*-axis denotes the first day of the correlation period (DOY), the *y*-axis denotes the period length of the correlation analysis result. The further from the top in the graph, the longer the period that is used in the correlation analysis. For example, at the very top, all days of the year are correlated with themselves. On the very left and going down, the first day of the year is correlated with all possible period lengths, for example between DOY 1 and 2, DOY 1 and 3 up to DOY 1 and DOY 365, at the very bottom of the graph

Temperature does not correlate significantly (i.e. $p < .1$) with TRW at this site for larch, and there is a slight significant negative correlation with higher temperatures and spruce TRW for the duration of about a month starting from DOY 145–153. The fact that temperature shows little to no significant correlation with ring widths at this site means that we do not have to account for it in our growth model, and can focus on soil moisture-driven growth processes.

3.3 | Growth period selection

To obtain a realistic growth period over which to parameterize the soil moisture growth-response function we used three sources of evidence (xylogenesis data, the daily-resolution climate correlation approach, and a growing degree-day model). For growth start t_1, the most common DOY (114) from the GDD-model of predicted growth onset across the century corresponded well with observations of xylogenesis data at DOY 118 for larch and 110 for spruce between 2008 and 2010. The end of growth (t_2) assessed through daily-resolution climate correlation was slightly later than xylogenesis observations by 7 and 8 days for larch and spruce respectively (Table 2), probably due to long lasting autocorrelation of daily Ψ_{soil} values.

3.4 | Optimization of the soil water-growth function

Using the selected growth period, observed TRWi chronologies and simulated soil moisture, we calibrated the soil water-growth response function. The optimum parameter combinations for Equations (1) and (3) together with their goodness-of-fit metric are summarized in Table 3. The optimized soil moisture response curve shape and additive growth model was able to reproduce 62.3% of the variation for larch and 59.4% of the variation for spruce of observed binned TRWi values (Figure 5d,h). Other intermediate steps, as well as upper and lower boundaries of the optimization, are also visualized in Figure 5. Figure 5b and g show

TABLE 2 Ring width increment start and end (DOY) from various sources in larch and spruce. Xylogenesis-derived periods are used for subsequent modelling steps. GDD-model and daily-resolution correlation analysis dates act as additional evidence to the xylogenesis-derived dates' applicability for simulations throughout the century

	Xylogenesis		GDD	Daily-resolution correlation	Final critical period in dates
Species	Start	End	Start	End	
Larch	118	183	114	190	27 April–1 July
Spruce	110	190	114	198	9 April–8 July

TABLE 3 Optimized species-specific soil water-growth function parameters ψ_{crit} and their ranges, together with their respective model-evaluation metric and auxillary parameter a, a scaling coefficient. ψ_{crit} is the optimized parameter value of the soil water-growth function. ψ_{crit} minimum and maximum values are the upper and lower bound of the range for which we identified $R^2(a^*)$ to be >0 under varying ψ_{crit} parameters. a^* is the optimized scaling coefficient. R^2 (more precisely $R^2(a^*)$) is the maximum variance reproduced between observed $TRWi_b$ values and final TRWs (Equation 3), which were simulated using our proposed model relationship between Ψ_{soil} histories

Species	Optimum ψ_{crit}	ψ_{crit} min	ψ_{crit} max	a^*	R^2
Larch	−0.47 MPa	−1.4 MPa	−0.24 MPa	0.0244	.624
Spruce	−0.66 MPa	−1.4 MPa	−0.38 MPa	0.0170	.594

Abbreviation: TRW, tree ring width.

R^2 and $R^2(a^*)$ dynamics with decreasing ψ_{crit} parameter, in search of the maximum R^2. R^2 values under decreasing ψ_{crit} first increase steeply until the maximum value of 0.624 for larch and 0.594 for spruce, and then deteriorate gradually to 0.4660 for larch and 0.4150 for spruce at −4.6 MPa (not shown). Using the optimized scaling coefficient a^*, $R^2(a^*)$ first increases and then declines steeply under different decreasing ψ_{crit}. R^2 and $R^2(a^*)$ share the same optimum, as they share the same scaling coefficient at that point.

Figure 5c and g show a range of soil moisture growth response curves (modelled with constant a^*), colour-coded by their ability to reproduce a large relative proportion (>50%) of variance when used to simulate TRWs. The beta-response curve with the highest proportion of variance reproduced is highlighted in yellow and has x-intercepts corresponding to the optimized ψ_{crit} of −0.47 MPa for larch and −0.66 MPa for spruce.

3.5 | Source–sink response function comparison

Source versus sink-type responses to soil or leaf water potential are shown in Figure 6. Typical source response functions as currently implemented in DGVMs are shown in (a) and (b), together with the sink response functions derived in this study.

Our sink responses are put in context with observed source and sink-type responses to soil or leaf water potential in Figure 6b. The pair of source and sink functions for each species that emerges from Figure 6b shows that the sink is always more limited than the source as soil or leaf water potential declines (see Muller et al., 2011, for more such functions). Besides, while the source responses differ in shape (both in the models and the observations), the sink-type responses all abruptly decline, which makes them more similar to one another. This study's sink-type response function calibrated to two different species is similar to the observed sink-type responses in two crops and mature evergreen oaks (Figure 6b).

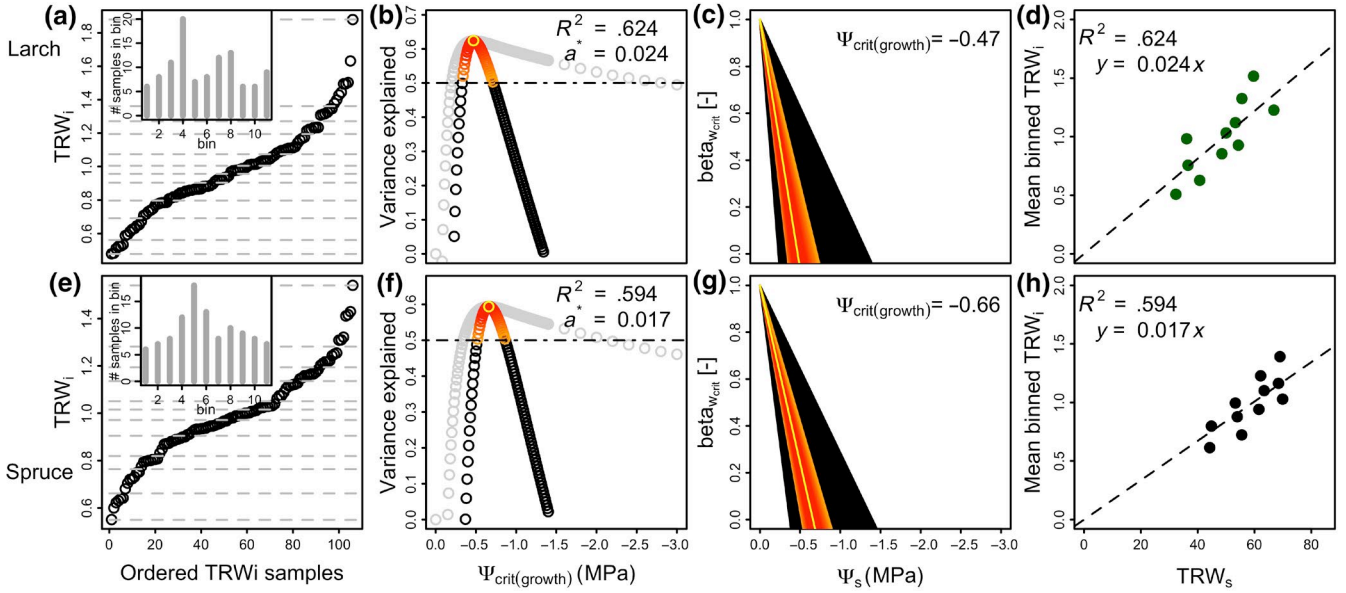

FIGURE 5 (a)/(e) Bin placements for clustered binning, with 11 bins and the distribution of the number of tree ring width index (TRWi) samples within the bins. (b)/(f) Evolution of R^2 (grey dots) and R^2(a*) values (black, orange and red dots), given different ψ_{crit} thresholds for both and slope (*a*) values for R^2. The optimized parameter a^* is fixed for the calculation of the R^2(a*) under different ψ_{crit}. Values above 0 mean that the response curve together with the growth model can reproduce more than the average observations. Values above 0.5 and approaching 1 indicate a close match between TRWs and observed TRW (orange to red). (c)/(g) Soil water-growth response curves, with different values of ψ_{crit} (=*x*-intercepts). Orange-red is the collection of response functions which generate R^2(a*) values above 0.5 (see panels b and f). The yellow line is the optimal beta-response curve, giving the best fit between TRWi and TRWs (equivalent to the *x*-axis location of the maximum R^2 and R^2[a*] in [b] and [f]). (d)/(h) Observed mean of the binned TRW_i (as displayed in panels a and e) are plotted against the best-fit growth model output (TRW_s; with optimized values of ψ_{crit} = −0.47 MPa for larch or −0.66 MPa for spruce) and the proportion of variance reproduced by each model

4 | DISCUSSION

Detailed knowledge on the relationship between TRW increment and soil water content is currently limited to a very few studies, which are all on drought-adapted species using short-term experiments under non-natural growth conditions. With projected increase in hydrological stress in many ecosystems of the world, we require a deeper understanding of soil moisture growth responses in order to accurately predict tree growth in a drying world. To address this issue, we combined TRW chronologies and modelled soil moisture dynamics to parameterize a soil water-growth response curve. We found a very strong and immediate response of modelled ring increment to simulated soil water, with growth cessation in the wet range of soil water potential (−0.47 MPa for larch and −0.66 MPa for spruce), consistent with existing observations on trees (Bogeat-Triboulot et al., 2007; Lempereur et al., 2015). This response curve can be directly used in the modelling of tree ring increment in DGVMs in response to soil moisture variations. These findings have profound implications for the modelling of growth and thus carbon incorporation into biomass and hence predictions of vegetation carbon pool dynamics.

Comparing our new data-derived soil moisture growth-relationship with existing soil moisture stomatal conductance and photosynthesis response curves from models and observations demonstrates that the carbon input to trees is much less sensitive to soil moisture reductions than growth increment, thus supporting the sink-limitation hypothesis (Körner, 2015; Sweet & Wareing, 1966). Ultimately, the source and sink probably interact to form a functional equilibrium in the long term (Zweifel et al., 2006), which still remains to be tested through balanced source–sink modelling (Friend et al., 2019).

This study increases our knowledge on tree ring growth response to soil moisture, contributes to the source–sink debate and provides thresholds for carbon allocation or bottom-up growth modelling in DGVMs. Our findings are a first step towards a currently lacking, broadly applicable model structure to represent tree ring growth processes in DGVMs (Babst et al., 2018).

4.1 | HYBRID9 model evaluation

In order to obtain realistic soil moisture growth response curves, we first had to verify the robustness of the HYBRID9 hydrology framework, which provides the simulated soil moisture across the century, necessary for our analysis. We found that HYBRID9 is able to capture inter- and intra-annual dynamics of soil moisture well in both observed layers, and there is no consistent pattern of seasonal bias in soil moisture at the studied site during the observational period. A good agreement between observed and simulated soil moisture dynamics and between modelled total surface evapotranspiration and the MODIS ET product make us conclude that HYBRID9 hydrology is robust at this site. The verified hydrology gives us confidence in the century-long simulated soil moisture time series used for deriving the soil moisture response curve.

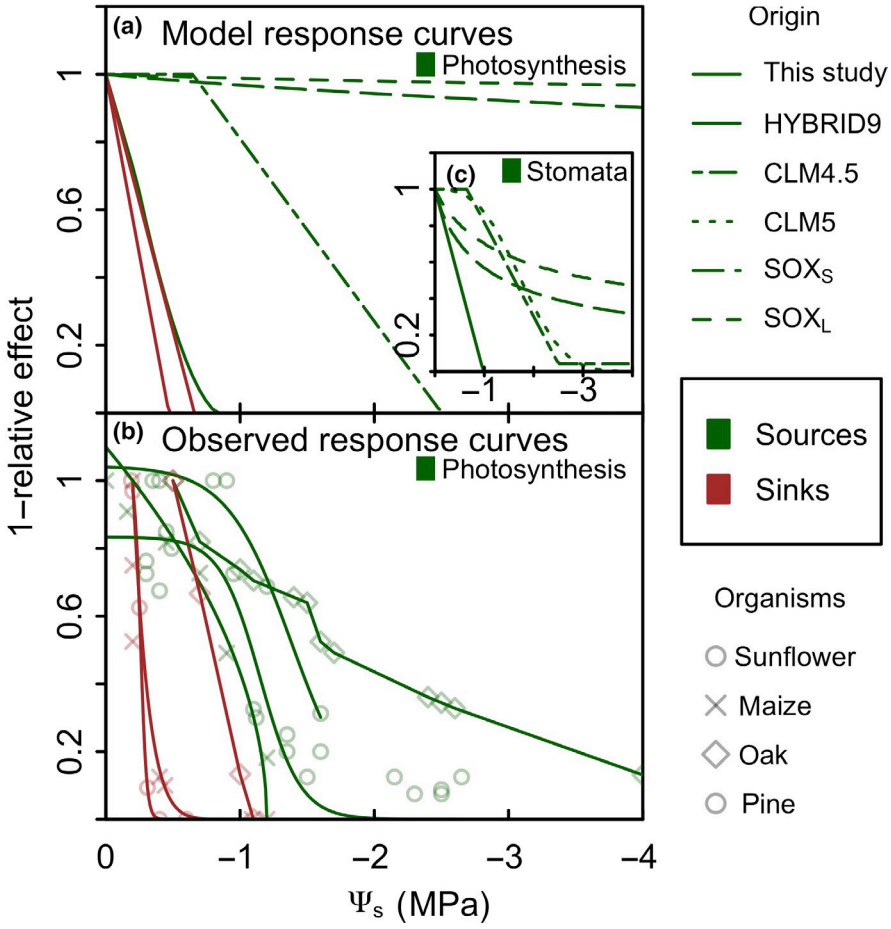

FIGURE 6 Source (green) versus sink (brown) type responses to soil or leaf water potential. (a) Sink (stem growth increment) response curves derived from this study and source (photosynthesis) response curves for varying soil or leaf water potential suggested for or in some current dynamic global vegetation models (DGVMs). (b) Source and sink responses to soil or leaf water potential in observational studies. (c) Source (stomatal conductance) response curves for varying soil or leaf water potential suggested for or in some current DGVMs. Sink responses different from the source-response curves are lacking in current DGVMs and can hence not be included. Results for sunflower and maize are from Boyer (1970), with measurements of leaf water potential. Source responses are based on normalized photosynthesis measurements. Sink responses are normalized growth, measured as leaf enlargement rates. Results from mature oak are based on a field study with rainfall exclusion (Lempereur et al., 2015), where source responses are based on normalized GPP measured from eddy covariance carbon fluxes, and sink responses are based on normalized change in basal area increment under simulated predawn soil water potential. Pine results are mean values of four 3 year old *Pinus nigra* saplings (varieties pooled) from Lebourgeois et al. (1998) in droughted plots. HYBRID9: Bounded-linear beta-response curve (see CLM4.5) used to simulate soil moisture dynamics in this study, with default threshold parameter −1 MPa. The beta-factor is applied directly to stomatal openness, which modifies C_i, and in the Farquhar–von Caemmerer–Berry-type photosynthesis model on V_{cmax}, J_{max} and respiration (Farquhar et al.,1980). In CLM4.5 soil moisture directly affects stomatal openness which is described using the Ball-Berry conductance model (Collatz et al., 1991), and impacts photosynthesis through the soil moisture stress factor on V_{cmax} and respiration. In CLM5 the sigmoidally shaped water stress effect on stomatal conductance is included through dynamically varying leaf water potential. Photosynthesis is not included. Stomatal optimisation model based on xylem hydraulics (SOX): The emergent curve from the stomatal optimization model (Eller et al., 2018), includes a xylem hydraulic conductivity cost, while maximizing gross photosynthesis (Eller et al., 2018). SOX_L and SOX_S differ only by using larch P50 and spruce P50 values as hydraulic conductivity parameters respectively (Rosner et al., 2019). All models are run with default plant type/species-specific parameters; adjusted parameters are in Table S5. Stomatal conductance and photosynthesis are modelled as coupled system in HYBRID9, CLM4.5 and SOX. See also model-specific grouping of stomatal conductance and photosynthesis response curves in Figure S10

4.2 | Comparison of the parameterized growth function to observed growth responses

Growth response curve shape and cessation threshold values ψ_{crit} (−0.47 MPa for larch and −0.66 MPa for spruce) produced in this study are similar to other studies on soil moisture impacts on vegetative growth. Studies on the relationship between soil moisture and sunflower shoot growth (Sionit et al., 1973) and holm oak stem increment (Lempereur et al., 2015) did not find evidence for a threshold above which soil water does not affect growth. This matches the immediately declining growth response curve from saturated soil in this study. Growth cessation thresholds were reported

between −0.2 MPa (Green et al., 1971) in *Nitella* internodes, in the range of −0.43 to −0.6 MPa for sunflower (Sionit et al., 1973), −0.7 to −0.8 MPa for maize (Boyer, 1970) and −1.1 MPa for holm oak (Lempereur et al., 2015). All these values are within our lower predicted boundary of Ψ_{soil} values (−1.4 MPa for both larch and spruce). The lowest observed threshold in holm oak could be caused by oaks having a larger water store than corn, sunflower, larch or spruce, of which the latter two store water mainly in branches (Schulze et al., 1985). Overall, despite a broad range of species, growth threshold values in the literature and from our study span similar ranges.

4.3 | Mechanisms and drivers involved in growth increment dynamics

The mechanisms underlying the soil moisture response curve shape found in this study could involve hydraulic factors, hormonal factors or a combination of these. In the literature it is unclear whether it is mainly the loss of turgor pressure (Ogawa & Yamauchi, 2006), an abscisic acid (ABA)-regulated decrease in cell wall extensibility (Gimeno-Gilles et al., 2009) or an interplay of both at different timescales and drought severity levels (Van Volkenburgh & Cleland, 1986) that is the mechanism behind our response function. From a hydraulic perspective, a threshold below which enlargement could not be overcome through osmotic adjustment was −0.41 MPa in maize seedling root cells (Ogawa & Yamauchi, 2006). This threshold is close to the soil moisture values below which growth ceases in our study (−0.47 and −0.66 MPa). From a hormonal perspective, it has been suggested that ABA impacts both cell proliferation and expansion (Hsiao, 1973; Jenkins & Shepherd, 1974; Wodzicki & Wodzicki, 1980) but evidence for the former is not very strong (Luisi et al., 2014). The similarity in observed growth response and threshold ranges between species (see Figure 6 and Ogawa & Yamauchi, 2006) seems to suggest a physical rather than a biological (signalling) constraint on growth in very water-constrained environments such as this site. More research, particularly on the long- and short-term between interplay between hormonal and hydraulic dynamics in stem growth under soil moisture stress, is needed.

Besides water, temperature is known to influence wood formation, both in terms of phenology and growth rate. Growth start has been found to be largely temperature-dependent (Delpierre et al., 2018; Huang et al., 2020; Oribe & Funada, 2017; Rossi et al., 2016) and using the temperature-based CLM5.0 GDD-model to simulate growth start worked well in confirming a likely t_1 for our site. This implies that temperature may be involved in growth onset at our site to some degree, even though the daily-resolution correlation analysis did not find a significant temperature-effect on TRWi early in the year. Photoperiod or temperature were dismissed as sole drivers of growth cessation at this and nearby sites (Cuny et al., 2019), and we find that soil moisture is more important at our site and nearby (Eilmann et al., 2011). Temperature has been confirmed to influence cell production rates (e.g. Gričar et al., 2006; Ren et al., 2019) under non water-limiting conditions and it is likely that temperature has a complex and subtle role to play at our site. Indeed, it has been suggested that ongoing climate warming in this area (King et al., 2013) has made this and nearby sites less sensitive to direct growth limitations by temperature (Cabon et al., 2020), with maybe the exception of growth onset (Cuny et al., 2019). However, high temperatures probably act together with low precipitation to cause the observed drought-induced cessation or slowing of wood formation (Cabon et al., 2020; also seen in our soil moisture simulations), similar to Mediterranean systems (Cabon et al., 2018; Lempereur et al., 2017). Another indirect effect of temperature may have been to act on stem water potential via the influence on vapour pressure deficit. However, we tested whether temperature is not limiting at this site and found a lack of temperature influence on ring increment by observing that the remaining variability in TRWi was not correlated with any intra-annual (short term) fluctuations in temperature (daily-resolution correlation analysis). Nevertheless, (Cabon et al., 2020) show that including both temperature and stem water potential best replicates observed rates of cell production at nearby sites. We acknowledge that the optimized response curves cannot be used to reproduce all variability between TRWi and TRWs which is probably caused by the same growing season length for each simulated year, but possibly also due to temperature influences while soil water was non-limiting.

4.4 | A case for separate representations of source and sink processes

The high sensitivity of radial tree growth to soil moisture found here means that a wide range of soil moisture regimes still modulate the sources, while being too low for the growth sink (Bogeat-Triboulot et al., 2007; Boyer, 1970; Hummel et al., 2010; Lempereur et al., 2015; Tardieu et al., 1999; Wardlaw, 1990). This would imply that carbon availability would never be limiting to growth (Körner, 2003, 2006, 2015) which however is currently assumed in state-of-the-art DGVMs through the direct allocation of carbon to biomass (as fraction of gross primary productivity [GPP]). However, when resolving environmental impacts on carbon allocation to wood, Guillemot et al. (2017) show that their model CASTANEA can better predict aboveground forest growth in space and time. Likewise, Leuzinger et al. (2013) show that empirical modelling of a temperature impact on sink behaviour improved model fit to measurements of forest carbon and tree line position in the northern hemisphere. Besides different environmental sensitivities, different timings of source and sink activity throughout the season (Delpierre et al., 2016) also have important implications for modelling carbon allocation to biomass. On annual timescales, sources and sinks might correlate because their activities are modified by the same environmental drivers during a period of shared activity. However, GPP and growth are frequently not at all, or only weakly, correlated with one another on an intra-annual scale (Lempereur et al., 2015; Mund et al., 2010; but see Granier et al., 2008). Another more mechanistic reason for separate representation of these two processes is that internal coupling between source and sink processes may be necessary

to achieve overall homeostasis (e.g. leaf area −conducting xylem area; Zweifel et al., 2006), even if one process is ultimately more constrained by environmental factors than the other. Besides, explicitly representing tree growth processes such as ring increment within a DGVM may also help in developing tree ring-based mortality algorithms (Cailleret et al., 2017), and provide bench-marking opportunities (Zuidema et al., 2018). Ultimately, we envisage that integrating separate source and sink approaches will contribute to reducing prevailing uncertainty (Arora et al., 2013; Friedlingstein, 2015) for modelling terrestrial carbon cycle responses to climate change.

4.5 | Implications of a response curve for modelling sinks

Response curves such as ours can readily be used in DGVMs, either for the environmental control on carbon allocation to downstream pools such as the stem or explicit modelling of growth processes. In either case it will have a major impact on the prediction of long-term carbon allocation in response to soil moisture variability than a purely source-driven approach (Fatichi et al., 2014; Körner, 2003, 2005, 2015). When growth slows or stops during water stress, there may be an initial build-up of excess photosynthate. However the dynamics of NSCs following or during water stress are difficult to interpret, being timescale-, species- and age/size- specific (Mencuccini et al., 2013; Sala et al., 2012). Our growth response curve will help in carbon allocation modelling studies by providing a treatment of the direct response of the growth sink to soil water constraints independently of the response of carbon uptake. It must be noted that our response curve has been used to model volume increment, and thus direct use for carbon allocation assumes that wood density (carbon content within the ring) is constant, which in very limiting years causes an underestimation of carbon allocation to the ring (Bouriaud et al., 2005, 2015). Our response curve is derived using daily timestepping, which is a temporal unit that can be quickly integrated into models. A daily step can resolve differences in source–sink activity related to phenology and environmental responses (e.g. Guillemot et al., 2015), while not being too computationally intensive. Due to its one-paramteric formulation, the function is suitably parsimonious to be readily used in global modelling approaches. Our response curve is directly relevant for trees with little or exhausted water storage potential. However, for trees with more water storage potential (e.g. Steppe et al., 2015), we hypothesize that the immediate decline in this function would benefit from updating to accommodate dynamics of water release from storage. With our framework provided here, widely available TRW data can be used for the calibration of response curves of other species in other environmentally limited ecosystems. An appropriate first-order representation of growth processes and their interaction with environmental impacts such as soil moisture has the potential to contribute to reducing uncertainties in vegetation response to changing climates and thus improve our predictions of future carbon cycle dynamics.

ACKNOWLEDGEMENTS

The authors thank two anonymous reviewers for their valuable feedback on both shaping the overall story and addressing the necessary details.

CONFLICT OF INTEREST

None declared.

AUTHOR CONTRIBUTION

A.H.E.-S. performed the analysis and wrote the first draft of the manuscript. E.T. reviewed the analysis code and verified the analytical methods. A.H.E.-S. and A.D.F. conceived the study. A.D.F. helped steer the project and interpretation of the results. P.F. and Y.C. contributed with data. All authors contributed to discussing the results and editing the manuscript.

DATA AVAILABILITY STATEMENT

Data and analysis code are available at https://doi.org/10.17863/CAM.57197.

ORCID

Annemarie H. Eckes-Shephard https://orcid.org/0000-0002-2453-3843
Egor Tiavlovsky https://orcid.org/0000-0001-7341-7198
Yizhao Chen https://orcid.org/0000-0002-9218-6679
Patrick Fonti https://orcid.org/0000-0002-7070-3292
Andrew D. Friend https://orcid.org/0000-0002-9029-1045

REFERENCES

Allen, C. D., Breshears, D. D., & McDowell, N. G. (2015). On underestimation of global vulnerability to tree mortality and forest die-off from hotter drought in the Anthropocene. *Ecosphere*, *6*(8), art129. https://doi.org/10.1890/ES15-00203.1

Amenu, G. G., & Kumar, P. (2008). A model for hydraulic redistribution incorporating coupled soil-root moisture transport. *Hydrology and Earth System Sciences*, *12*(1), 55–74. https://doi.org/10.5194/hess-12-55-2008

Arora, V. K., Boer, G. J., Friedlingstein, P., Eby, M., Jones, C. D., Christian, J. R., Bonan, G., Bopp, L., Brovkin, V., Cadule, P., & Hajima, T. (2013). Carbon-climate feedbacks in CMIP5 earth system models. *Journal of Climate*, *26*(15), 5289–5314. https://doi.org/10.1175/JCLI-D-12-00494.1

Babst, F., Bodesheim, P., Charney, N., Friend, A. D., Girardin, M. P., Klesse, S., Moore, D. J. P., Seftigen, K., Björklund, J., Bouriaud, O., Andria Dawson, R., DeRose, J., Dietze, M. C., Eckes, A. H., Enquist, B., Frank, D. C., Mahecha, M. D., Poulter, B., Record, S., … Evans, M. E. K. (2018). When tree rings go global: Challenges and opportunities for retro- and prospective insight. *Quaternary Science Reviews*, *197*, 1–20. https://doi.org/10.1016/j.quascirev.2018.07.009

Bogeat-Triboulot, M.-B., Brosché, M., Renaut, J., Jouve, L., Le Thiec, D., Fayyaz, P., Vinocur, B., Witters, E., Laukens, K., Teichmann, T., Altman, A., Hausman, J.-F., Polle, A., Kangasjärvi, J., & Dreyer, E. (2007). Gradual soil water depletion results in reversible changes of gene expression, protein profiles, ecophysiology, and growth performance in *Populus euphratica*, a poplar growing in arid regions. *Plant Physiology*, *143*(2), 876–892. https://doi.org/10.1104/pp.106.088708

Bouriaud, O., Leban, J.-M., Bert, D., & Deleuze, C. (2005). Intra-annual variations in climate influence growth and wood density of Norway

spruce. *Tree Physiology*, *25*(6), 651–660. https://doi.org/10.1093/treephys/25.6.651

Bouriaud, O., Teodosiu, M., Kirdyanov, A. V., & Wirth, C. (2015). Influence of wood density in tree-ring-based annual productivity assessments and its errors in Norway spruce. *Biogeosciences*, *12*(20), 6205–6217. https://doi.org/10.5194/bg-12-6205-2015

Boyer, J. S. (1970). Leaf enlargement and metabolic rates in corn, soybean, and sunflower at various leaf water potentials. *Plant Physiology*, *46*(2), 233–235. https://doi.org/10.1104/pp.46.2.233

Brzostek, E. R., Dragoni, D., Schmid, H. P., Rahman, A. F., Sims, D., Wayson, C. A., Johnson, D. J., & Phillips, R. P. (2014). Chronic water stress reduces tree growth and the carbon sink of deciduous hardwood forests. *Global Change Biology*, *20*(8), 2531–2539. https://doi.org/10.1111/gcb.12528

Cabon, A., Mouillot, F., Lempereur, M., Ourcival, J.-M., Simioni, G., & Limousin, J.-M. (2018). Thinning increases tree growth by delaying drought-induced growth cessation in a Mediterranean evergreen oak coppice. *Forest Ecology and Management*, *409*, 333–342. https://doi.org/10.1016/j.foreco.2017.11.030

Cabon, A., Peters, R. L., Fonti, P., Martínez-Vilalta, J., & De Cáceres, M. (2020). Temperature and water potential co-limit stem cambial activity along a steep elevational gradient. *New Phytologist*, *226*(5), 1325–1340. https://doi.org/10.1111/nph.16456

Cailleret, M., Jansen, S., Robert, E. M. R., Desoto, L., Aakala, T., Antos, J. A., Beikircher, B., Bigler, C., Bugmann, H., Caccianiga, M., Čada, V., Camarero, J. J., Cherubini, P., Cochard, H., Coyea, M. R., Čufar, K., Das, A. J., Davi, H., Delzon, S., … Martínez-Vilalta, J. (2017). A synthesis of radial growth patterns preceding tree mortality. *Global Change Biology*, *23*(4), 1675–1690. https://doi.org/10.1111/gcb.13535

Collatz, G. J., Ball, J. T., Grivet, C., & Berry, J. A. (1991). Physiological and environmental regulation of stomatal conductance, photosynthesis and transpiration: A model that includes a laminar boundary layer. *Agricultural and Forest Meteorology*, *54*(2–4), 107–136. https://doi.org/10.1016/0168-1923(91)90002-8

Crowther, T. W., Glick, H. B., Covey, K. R., Bettigole, C., Maynard, D. S., Thomas, S. M., Smith, J. R., Hintler, G., Duguid, M. C., Amatulli, G., Tuanmu, M.-N., Jetz, W., Salas, C., Stam, C., Piotto, D., Tavani, R., Green, S., Bruce, G., Williams, S. J., … Bradford, M. A. (2015). Mapping tree density at a global scale. *Nature*, *525*(7568), 201–205. https://doi.org/10.1038/nature14967

Cuny, H. E., Fonti, P., Rathgeber, C. B. K., von Arx, G., Peters, R. L., & Frank, D. C. (2019). Couplings in cell differentiation kinetics mitigate air temperature influence on conifer wood anatomy. *Plant, Cell & Environment*, *42*(4), 1222–1232. https://doi.org/10.1111/pce.13464

Cuny, H. E., Rathgeber, C. B. K., Frank, D., Fonti, P., Mäkinen, H., Prislan, P., Rossi, S., Martinez, E., del Castillo, F., Campelo, H. V., Camarero, J. J., Bryukhanova, M. V., Jyske, T., Gričar, J., Gryc, V., De Luis, M., Vieira, J., Čufar, K., Kirdyanov, A. V., … Fournier, M. (2015). Woody biomass production lags stem-girth increase by over one month in coniferous forests. *Nature Plants*, *1*(11). https://doi.org/10.1038/nplants.2015.160

Cuny, H. E., Rathgeber, C. B. K., Lebourgeois, F., Fortin, M., & Fournier, M. (2012). Life strategies in intra-annual dynamics of wood formation: Example of three conifer species in a temperate forest in north-east France. *Tree Physiology*, *32*(5), 612–625. https://doi.org/10.1093/treephys/tps039

Delpierre, N., Berveiller, D., Granda, E., & Dufrêne, E. (2016). Wood phenology, not carbon input, controls the interannual variability of wood growth in a temperate oak forest. *New Phytologist*, *210*(2), 459–470. https://doi.org/10.1111/nph.13771

Delpierre, N., Lireux, S., Florian Hartig, J., Camarero, J., Cheaib, A., Čufar, K., Cuny, H., Deslauriers, A., Fonti, P., Gričar, J., Huang, J.-G., Krause, C., Liu, G., de Luis, M., Mäkinen, H., Martinez, E., del Castillo, H., Morin, P. N., Oberhuber, W., … Rathgeber, C. B. K. (2018). Chilling and forcing temperatures interact to predict the onset of wood formation in Northern Hemisphere conifers. *Global Change Biology*, *25*, 1089–1105. https://doi.org/10.1111/gcb.14539

Douglass, A. E. (1914). A method of estimating rainfall by the growth of trees. *Bulletin of the American Geographical Society*, *46*(5), 321–335. https://doi.org/10.2307/201814

Downes, G., Beadle, C., & Worledge, D. (1999). Daily stem growth patterns in irrigated *Eucalyptus globulus* and *E. nitens* in relation to climate. *Trees*, *14*(2), 102–111. https://doi.org/10.1007/PL00009752

Eilmann, B., Zweifel, R., Buchmann, N., Pannatier, E. G., & Rigling, A. (2011). Drought alters timing, quantity, and quality of wood formation in Scots pine. *Journal of Experimental Botany*, *62*(8), 2763–2771. https://doi.org/10.1093/jxb/erq443

Ekici, A., Chadburn, S., Chaudhary, N., Hajdu, L. H., Marmy, A., Peng, S., Boike, J., Burke, E., Friend, A. D., Hauck, C., Krinner, G., Langer, M., Miller, P. A., & Beer, C. (2015). Site-level model intercomparison of high latitude and high altitude soil thermal dynamics in tundra and barren landscapes. *The Cryosphere*, *9*(4), 1343–1361. https://doi.org/10.5194/tc-9-1343-2015

Eller, C. B., Rowland, L., Oliveira, R. S., Bittencourt, P. R. L., Barros, F. V., da Costa, A. C. L., Meir, P., Friend, A. D., Mencuccini, M., Sitch, S., & Cox, P. (2018). Modelling tropical forest responses to drought and El Niño with a stomatal optimization model based on xylem hydraulics. *Philosophical Transactions of the Royal Society B: Biological Sciences*, *373*(1760), 20170315. https://doi.org/10.1098/rstb.2017.0315

Farquhar, G. D., von Caemmerer, S., & Berry, J. A. (1980). A biochemical model of photosynthetic CO_2 assimilation in leaves of C3 species. *Planta*, *149*(1), 78–90. https://doi.org/10.1007/BF00386231

Fatichi, S., Leuzinger, S., & Körner, C. (2014). Moving beyond photosynthesis: From carbon source to sink-driven vegetation modeling. *New Phytologist*, *201*(4), 1086–1095. https://doi.org/10.1111/nph.12614

Fatichi, S., Pappas, C., Zscheischler, J., & Leuzinger, S. (2019). Modelling carbon sources and sinks in terrestrial vegetation. *New Phytologist*, *221*(2), 652–668. https://doi.org/10.1111/nph.15451

Friedlingstein, P. (2015). Carbon cycle feedbacks and future climate change. *Philosophical Transactions of the Royal Society A: Mathematical, Physical and Engineering Sciences*, *373*(2054), 1471–2962. https://doi.org/10.1098/rsta.2014.0421

Friend, A. D., Eckes-Shephard, A. H., Fonti, P., Rademacher, T. T., Rathgeber, C. B. K., Richardson, A. D., & Turton, R. H. (2019). On the need to consider wood formation processes in global vegetation models and a suggested approach. *Annals of Forest Science*, *76*(2), 49. https://doi.org/10.1007/s13595-019-0819-x

Friend, A. D., Stevens, A. K., Knox, R. G., & Cannell, M. G. R. (1997). A process-based, terrestrial biosphere model of ecosystem dynamics (Hybrid v3.0). *Ecological Modelling*, *95*(2–3), 249–287. https://doi.org/10.1016/S0304-3800(96)00034-8

Génard, M., Fishman, S., Vercambre, G., Huguet, J.-G., Bussi, C., Besset, J., & Habib, R. (2001). A biophysical analysis of stem and root diameter variations in woody plants. *Plant Physiology*, *126*(1), 188–202. https://doi.org/10.1104/pp.126.1.188

Gimeno-Gilles, C., Lelièvre, E., Viau, L., Malik-Ghulam, M., Ricoult, C., Niebel, A., Leduc, N., & Limami, A. M. (2009). ABA mediated inhibition of germination is related to the inhibition of genes encoding cell-wall biosynthetic and architecture: Modifying enzymes and structural proteins in *Medicago truncatula* embryo axis. *Molecular Plant*, *2*(1), 108–119. https://doi.org/10.1093/mp/ssn092

Giovannelli, A., Deslauriers, A., Fragnelli, G., Scaletti, L., Castro, G., Rossi, S., & Crivellaro, A. (2007). Evaluation of drought response of two poplar clones (*Populus* × *canadensis* Mönch 'I-214' and *P. deltoides* Marsh. 'Dvina') through high resolution analysis of stem growth. *Journal of Experimental Botany*, *58*(10), 2673–2683. https://doi.org/10.1093/jxb/erm117

Granier, A., Breda, N., Longdoz, B., Gross, P., & Ngao, J. (2008). Ten years of fluxes and stand growth in a young beech forest at Hesse,

North-eastern France. *Annals of Forest Science*, *65*(7), 704. https://doi.org/10.1051/forest:2008052

Green, P. B., Erickson, R. O., & Buggy, J. (1971). Metabolic and physical control of cell elongation rate. *Plant Physiology*, *47*(3), 423–430. https://doi.org/10.1104/pp.47.3.423

Gričar, J., Zupančič, M., Čufar, K., Koch, G., Schmitt, U., & Oven, P. Effect of local heating and cooling on cambial activity and cell differentiation in the stem of Norway Spruce (*Picea abies*). *Annals of Botany*, *97*(6), 943–951. https://doi.org/10.1093/aob/mcl050

Grissino-Mayer, H. D. (2001). Evaluating crossdating accuracy: A manual and tutorial for the computer program COFECHA. *Tree-Ring Research*, *57*, 205–221.

Guillemot, J., Francois, C., Hmimina, G., Dufrêne, E., Martin-StPaul, N. K., Soudani, K., Marie, G., Ourcival, J.-M., & Delpierre, N. (2017). Environmental control of carbon allocation matters for modelling forest growth. *New Phytologist*, *214*(1), 180–193. https://doi.org/10.1111/nph.14320

Guillemot, J., Martin-StPaul, N. K., Dufrêne, E., François, C., Soudani, K., Ourcival, J. M., & Delpierre, N. (2015). The dynamic of the annual carbon allocation to wood in European tree species is consistent with a combined source–sink limitation of growth: Implications for modelling. *Biogeosciences*, *12*(9), 2773–2790. https://doi.org/10.5194/bg-12-2773-2015

Hölttä, T., Makinen, H., Nojd, P., Makela, A., & Nikinmaa, E. (2010). A physiological model of softwood cambial growth. *Tree Physiology*, *30*(10), 1235–1252. https://doi.org/10.1093/treephys/tpq068

Hsiao, T. C. (1973). Plant responses to water stress. *Annual Review of Plant Physiology*, *24*(1), 519–570. https://doi.org/10.1146/annurev.pp.24.060173.002511

Huang, J.-G., Ma, Q., Rossi, S., Biondi, F., Deslauriers, A., Fonti, P., Liang, E., Mäkinen, H., Oberhuber, W., Rathgeber, C. B. K., Tognetti, R., Treml, V., Yang, B., Zhang, J.-L., Antonucci, S., Yves Bergeron, J., Camarero, J., Campelo, F., Čufar, K., … Ziaco, E. (2020). Photoperiod and temperature as dominant environmental drivers triggering secondary growth resumption in Northern Hemisphere conifers. *Proceedings of the National Academy of Sciences of the United States of America*, 1091–6490. https://doi.org/10.1073/pnas.2007058117

Hughes, M. K., Xiangding, W. U., Xuemei, S., & Garfin, G. M. (1994). A preliminary reconstruction of rainfall in North-Central China since A.D. 1600 from tree-ring density and width. *Quaternary Research*, *42*(1), 88–99. https://doi.org/10.1006/qres.1994.1056

Hummel, I., Pantin, F., Sulpice, R., Piques, M., Rolland, G., Dauzat, M., Christophe, A., Pervent, M., Bouteille, M., Stitt, M., Gibon, Y., & Muller, B. (2010). Arabidopsis plants acclimate to water deficit at low cost through changes of carbon usage: An integrated perspective using growth, metabolite, enzyme, and gene expression analysis. *Plant Physiology*, *154*(1), 357–372. https://doi.org/10.1104/pp.110.157008

Jenkins, P. A., & Shepherd, K. R. (1974). Seasonal changes in levels of indole-acetic acid and abscisic acid in stem tissues of *Pinus radiata*. *New Zealand Journal of Forestry Science*, *4*(3), 511–519.

Kaczka, R. J., Janecka, K., Hulist, A., & Spyt, B. (2017). Linking the growth/climate response of daily resolution with annual ring formation of Norway spruce in the Tatra Mountains. In M. Wistuba, A. Cedro, I. Malik, G. Helle, & H. Gärtner (Eds.), *TRACE – Tree rings in archaeology, climatology and ecology* (Vol. *15*, pp. 13–22). Scientific technical report STR 17/04, GFZ. German Research Centre for Geosciences.

Kharuk, V. I., Im, S. T., Petrov, I. A., Golyukov, A. S., Ranson, K. J., & Yagunov, M. N. (2017). Climate-induced mortality of Siberian pine and fir in the Lake Baikal Watershed, Siberia. *Forest Ecology and Management*, *384*, 191–199. https://doi.org/10.1016/j.foreco.2016.10.050

King, G. M., Gugerli, F., Fonti, P., & Frank, D. C. (2013). Tree growth response along an elevational gradient: Climate or genetics? *Oecologia*, *173*(4), 1587–1600. https://doi.org/10.1007/s00442-013-2696-6

Körner, C. (2003). Carbon limitation in trees. *Journal of Ecology*, *91*(1), 4–17. https://doi.org/10.1046/j.1365-2745.2003.00742.x

Körner, C. (2005). Carbon flux and growth in mature deciduous forest trees exposed to elevated CO_2. *Science*, *309*(5739), 1360–1362. https://doi.org/10.1126/science.111397

Körner, C. (2006). Plant CO_2 responses: An issue of definition, time and resource supply. *New Phytologist*, *172*(3), 393–411. https://doi.org/10.1111/j.1469-8137.2006.01886.x

Körner, C. (2015). Paradigm shift in plant growth control. *Current Opinion in Plant Biology*, *25*, 107–114. https://doi.org/10.1016/j.pbi.2015.05.003

Lawrence, D. M., Fisher, R. A., Koven, C. D., Oleson, K. W., Swenson, S. C., Bonan, G., Collier, N., Ghimire, B., Kampenhout, L., Kennedy, D., Kluzek, E., Lawrence, P. J., Li, F., Li, H., Lombardozzi, D., Riley, W. J., Sacks, W. J., Shi, M., Vertenstein, M., … Zeng, X. (2019). The Community Land Model Version 5: Description of New Features, Benchmarking, and Impact of Forcing Uncertainty. *Journal of Advances in Modeling Earth Systems*, *11*(12), 4245–4287. https://doi.org/10.1029/2018MS001583

Le Quéré, C., Andrew, R. M., Friedlingstein, P., Sitch, S., Hauck, J., Pongratz, J., Pickers, P. A., Korsbakken, J. I., Peters, G. P., Canadell, J. G., Arneth, A., Arora, V. K., Barbero, L., Bastos, A., Bopp, L., Chevallier, F., Chini, L. P., Ciais, P., Doney, S. C., … Zheng, B. O. (2018). Global carbon budget 2018. *Earth System Science Data*, *10*(4), 2141–2194. https://doi.org/10.5194/essd-10-2141-2018

Lempereur, M., Limousin, J.-M., Guibal, F., Ourcival, J.-M., Rambal, S., Ruffault, J., & Mouillot, F. (2017). Recent climate hiatus revealed dual control by temperature and drought on the stem growth of Mediterranean *Quercus ilex*. *Global Change Biology*, *23*(1), 42–55. https://doi.org/10.1111/gcb.13495

Lempereur, M., Martin-StPaul, N. K., Damesin, C., Joffre, R., Ourcival, J.-M., Rocheteau, A., & Rambal, S. (2015). Growth duration is a better predictor of stem increment than carbon supply in a Mediterranean oak forest: Implications for assessing forest productivity under climate change. *New Phytologist*, *207*(3), 579–590. https://doi.org/10.1111/nph.13400

Leuzinger, S., Manusch, C., Bugmann, H., & Wolf, A.. (2013). A sink-limited growth model improves biomass estimation along boreal and alpine tree lines. *Global Ecology and Biogeography*, *22*(8), 924–932. https://doi.org/10.1111/geb.12047

Ljungqvist, F. C., Piermattei, A., Seim, A., Krusic, P. J., Büntgen, U., He, M., Kirdyanov, A. V., Luterbacher, J., Schneider, L., Seftigen, K., Stahle, D. W., Villalba, R., Yang, B., & Esper, J. (2020). Ranking of tree-ring based hydroclimate reconstructions of the past millennium. *Quaternary Science Reviews*, *230*, 106074. https://doi.org/10.1016/j.quascirev.2019.106074

Luisi, A., Giovannelli, A., Traversi, M. L., Anichini, M., & Sorce, C. Hormonal responses to water deficit in cambial tissues of *Populus alba* L. *Journal of Plant Growth Regulation*, *33*(3), 489–498. https://doi.org/10.1007/s00344-013-9401-1

Mencuccini, M., Hölttä, T., Sevanto, S., & Nikinmaa, E. Concurrent measurements of change in the bark and xylem diameters of trees reveal a phloem-generated turgor signal. *New Phytologist*, *198*(4), 1143–1154. https://doi.org/10.1111/nph.12224

Merganičová, K., Merganič, J., Lehtonen, A., Vacchiano, G., Sever, M. Z. O., Augustynczik, A. L. D., Grote, R., Kyselová, I., Mäkelä, A., Yousefpour, R., Krejza, J., Collalti, A., & Reyer, C. P. O. (2019). Forest carbon allocation modelling under climate change. *Tree Physiology*. https://doi.org/10.1093/treephys/tpz105

Muller, B., Pantin, F., Génard, M., Turc, O., Freixes, S., Piques, M., & Gibon, Y. (2011). Water deficits uncouple growth from photosynthesis, increase C content, and modify the relationships between C and growth in sink organs. *Journal of Experimental Botany*, *62*(6), 1715–1729. https://doi.org/10.1093/jxb/erq438

Mund, M., Kutsch, W. L., Wirth, C., Kahl, T., Knohl, A., Skomarkova, M. V., & Schulze, E.-D. (2010). The influence of climate and fructification on the inter-annual variability of stem growth and net primary productivity in an old-growth, mixed beech forest. *Tree Physiology*, *30*(6), 689–704. https://doi.org/10.1093/treephys/tpq027

Ogawa, A., & Yamauchi, A. (2006). Root osmotic adjustment under osmotic stress in maize seedlings 1. Transient change of growth and water relations in roots in response to osmotic stress. *Plant Production Science*, *9*(1), 27–38. https://doi.org/10.1626/pps.9.27

Oleson, K., Lawrence, M., Bonan, B., Drewniak, B., Huang, M., Koven, D., Levis, S., Li, F., Thornton, E., Bozbiyik, A., Fisher, R., Heald, L., Kluzek, El., Lamarque, J.-F., Lawrence, J., Leung, R., Lipscomb, W., Muszala, P., Ricciuto, M., … Yang, Z.-L. (2013). *Technical description of version 4.5 of the Community Land Model (CLM)*. https://doi.org/10.5065/D6RR1W7M

Oribe, Y., & Funada, R. (2017). Locally heated dormant cambium can re-initiate cell production independently of new shoot growth in deciduous conifers (*Larix kaempferi*). *Dendrochronologia*, *46*, 14–23. https://doi.org/10.1016/j.dendro.2017.09.001

Pan, Y., Birdsey, R. A., Fang, J., Houghton, R., Kauppi, P. E., Kurz, W. A., Phillips, O. L., Shvidenko, A., Lewis, S. L., Canadell, J. G., Ciais, P., Jackson, R. B., Pacala, S. W., McGuire, A. D., Piao, S., Rautiainen, A., Sitch, S., & Hayes, D. (2011). A large and persistent carbon sink in the world's forests. *Science*, *333*(6045), 988–993. https://doi.org/10.1126/science.1201609

Rathgeber, C. B. K., Longuetaud, F., Mothe, F., Cuny, H., & Le Moguédec, G. (2011). Phenology of wood formation: Data processing, analysis and visualisation using R (package CAVIAR). *Dendrochronologia*, *29*(3), 139–149. https://doi.org/10.1016/j.dendro.2011.01.004

Rosner, S., Heinze, B., Savi, T., & Dalla-Salda, G. (2019). Prediction of hydraulic conductivity loss from relative water loss: New insights into water storage of tree stems and branches. *Physiologia Plantarum*, *165*(4), 843–854. https://doi.org/10.1111/ppl.12790

Running, S., Mu, Q., & Zhao, M. (2017). *MOD16A2 MODIS/Terra net evapotranspiration 8-day L4 global 500m SIN grid V006*. NASA EOSDIS Land Processes DAAC. https://doi.org/10.5067/MODIS/MOD16A2.006

Peters, R. L., Speich, M., Pappas, C., Kahmen, A., Arx, G., Graf Pannatier, E., Steppe, K., Treydte, K., Stritih, A., & Fonti, P. (2019). Contrasting stomatal sensitivity to temperature and soil drought in mature alpine conifers. *Plant, Cell & Environment*, *42*(5), 1674–1689. https://doi.org/10.1111/pce.13500

Ren, P., Ziaco, E., Rossi, S., Biondi, F., Prislan, P., & Liang, E. (2019). Growth rate rather than growing season length determines wood biomass in dry environments. *Agricultural and Forest Meteorology*, *271*, 46–53. https://doi.org/10.1016/j.agrformet.2019.02.031

Rossi, S., Anfodillo, T., Čufar, K., Cuny, H. E., Deslauriers, A., Fonti, P., Frank, D., Gričar, J., Gruber, A., Huang, J.-G., Jyske, T., Kašpar, J., King, G., Krause, C., Liang, E., Mäkinen, H., Morin, H., Nöjd, P., Oberhuber, W., … Treml, V. (2016). Pattern of xylem phenology in conifers of cold ecosystems at the Northern Hemisphere. *Global Change Biology*, *22*(11), 3804–3813. https://doi.org/10.1111/gcb.13317

Sala, A., Woodruff, D. R., & Meinzer, F. C. (2012). Carbon dynamics in trees: Feast or famine? *Tree Physiology*, *32*(6), 764–775. https://doi.org/10.1093/treephys/tpr143

Schenk, H. J., & Jackson, R. B. (2002). The global biogeography of roots. *Ecological Monographs*, *72*(3), 311–328. https://doi.org/10.1890/0012-9615(2002)072[0311:TGBOR]2.0.CO;2

Schulze, E.-D., Čermák, J., Matyssek, R., Penka, M., Zimmermann, R., Vasícek, F., Gries, W., & Kučera, J. (1985). Canopy transpiration and water fluxes in the xylem of the trunk of larix and picea trees: A comparison of xylem flow, porometer and cuvette measurements. *Oecologia*, *66*(4), 475–483. https://doi.org/10.1007/bf00379337

Shuttleworth, W. J., & Wallace, J. S. (1985). Evaporation from sparse crops – An energy combination theory. *Quarterly Journal – Royal Meteorological Society*, *111*, 839–855. https://doi.org/10.1002/qj.49711146910

Sionit, N., Ghorashy, S. R., & Kheradnam, M. (1973). Effect of soil water potential on growth and yield of sunflower (*Helianthus annuus*). *The Journal of Agricultural Science*, *81*(1), 113–116. https://doi.org/10.1017/S002185960005838X

Steppe, K., De Pauw, D. J. W., Lemeur, R., & Vanrolleghem, P. A. (2006). A mathematical model linking tree sap flow dynamics to daily stem diameter fluctuations and radial stem growth. *Tree Physiology*, *26*(3), 257–273. https://doi.org/10.1093/treephys/26.3.257

Steppe, K., Sterck, F., & Deslauriers, A. (2015). Diel growth dynamics in tree stems: Linking anatomy and ecophysiology. *Trends in Plant Science*, *20*(6), 335–343. https://doi.org/10.1016/j.tplants.2015.03.015

Sweet, G. B., & Wareing, P. F. (1966). Role of plant growth in regulating photosynthesis. *Nature*, *210*(5031), 77–79. https://doi.org/10.1038/210077a0

Tardieu, F., Granier, C., & Muller, B. (1999). Modelling leaf expansion in a fluctuating environment: Are changes in specific leaf area a consequence of changes in expansion rate? *New Phytologist*, *143*(1), 33–43. https://doi.org/10.1046/j.1469-8137.1999.00433.x

Van Volkenburgh, E., & Cleland, R. E. (1986). Wall yield threshold and effective turgor in growing bean leaves. *Planta*, *167*(1), 37–43. https://doi.org/10.1007/BF0044636

Viovy, N. (2018). *CRUNCEP version 7 – Atmospheric forcing data for the community land model*. https://doi.org/10.5065/PZ8F-F017

Wardlaw, I. F. (1990). Tansley review no. 27: The control of carbon partitioning in plants. *New Phytologist*, *116*(3), 341–381. https://doi.org/10.1111/j.1469-8137.1990.tb00524.x

Wodzicki, T. J., & Wodzicki, A. B. (1980). Seasonal abscisic acid accumulation in stem cambial region of *Pinus silvestris*, and its contribution to the hypothesis of a late-wood control system in conifers. *Physiologia Plantarum*, *48*(3), 443–447. https://doi.org/10.1111/j.1399-3054.1980.tb03283.x

Zeng, X., & Decker, M. (2009). Improving the numerical solution of soil moisture-based richards equation for land models with a deep or shallow water table. *Journal of Hydrometeorology*, *10*(1), 308–319. https://doi.org/10.1175/2008JHM1011.1

Zuidema, P. A., Poulter, B., & Frank, D. C. (2018). A wood biology agenda to support global vegetation modelling. *Trends in Plant Science*, *23*(11), 1006–1015. https://doi.org/10.1016/j.tplants.2018.08.003

Zweifel, R., Zimmermann, L., Zeugin, F., & David, M. (2006). Newbery. Intra-annual radial growth and water relations of trees: Implications towards a growth mechanism. *Journal of Experimental Botany*, *57*(6), 1445–1459. https://doi.org/10.1093/jxb/erj125

SUPPORTING INFORMATION

Additional supporting information may be found online in the Supporting Information section.

How to cite this article: Eckes-Shephard AH, Tiavlovsky E, Chen Y, Fonti P, Friend AD. Direct response of tree growth to soil water and its implications for terrestrial carbon cycle modelling. *Glob Change Biol*. 2021;27:121–135. https://doi.org/10.1111/gcb.15397